NRC Publications Archive
Archives des publications du CNRC

Versatile microwave photonic signal processor based on a quantum-dash mode-locked laser

Wang, Zhuoran; Xie, Yuxuan; Wang, Xi; Wei, Zixian; Zhang, Jinsong; Liu, Jiaren; Lu, Zhenguo; Poole, Philip J.; Weber, John; Liu, Guocheng; Rahim, Mohamed; Plant, David V.; Chen, Lawrence R.

This publication could be one of several versions: author's original, accepted manuscript or the publisher's version. / La version de cette publication peut être l'une des suivantes : la version prépublication de l'auteur, la version acceptée du manuscrit ou la version de l'éditeur.

For the publisher's version, please access the DOI link below./ Pour consulter la version de l'éditeur, utilisez le lien DOI ci-dessous.

Publisher's version / Version de l'éditeur:

https://doi.org/10.1109/JLT.2025.3573682

Journal of Lightwave Technology, pp. 1-8, 2025-05-27

NRC Publications Archive Record / Notice des Archives des publications du CNRC :

https://nrc-publications.canada.ca/eng/view/object/?id=b83183f2-105b-4274-b512-0d4cc4f6d814
https://publications-cnrc.canada.ca/fra/voir/objet/?id=b83183f2-105b-4274-b512-0d4cc4f6d814

Access and use of this website and the material on it are subject to the Terms and Conditions set forth at
https://nrc-publications.canada.ca/eng/copyright
READ THESE TERMS AND CONDITIONS CAREFULLY BEFORE USING THIS WEBSITE.

L'accès à ce site Web et l'utilisation de son contenu sont assujettis aux conditions présentées dans le site
https://publications-cnrc.canada.ca/fra/droits
LISEZ CES CONDITIONS ATTENTIVEMENT AVANT D'UTILISER CE SITE WEB.

Questions? Contact the NRC Publications Archive team at PublicationsArchive-ArchivesPublications@nrc-cnrc.gc.ca. If you wish to email the authors directly, please see the first page of the publication for their contact information.

Vous avez des questions? Nous pouvons vous aider. Pour communiquer directement avec un auteur, consultez la première page de la revue dans laquelle son article a été publié afin de trouver ses coordonnées. Si vous n'arrivez pas à les repérer, communiquez avec nous à PublicationsArchive-ArchivesPublications@nrc-cnrc.gc.ca.

National Research Council Canada
Conseil national de recherches Canada

This article has been accepted for publication in Journal of Lightwave Technology. This is the author's version which has not been fully edited and content may change prior to final publication. Citation information: DOI 10.1109/JLT.2025.3573682

Versatile microwave photonic signal processor based on a quantum-dash mode-locked laser

Zhuoran Wang, Yuxuan Xie, Xi Wang, Zixian Wei, Jinsong Zhang, Jiaren Liu, Zhenguo Lu, Philip J. Poole, John Weber, Guocheng Liu, Mohamed Rahim, David V. Plant, *Fellow, IEEE*, and Lawrence R. Chen, *Senior Member, IEEE*

***Abstract*—Microwave photonic (MWP) signal processing offers the advantage of large time-bandwidth capability to overcome the inherent limitations of electronic systems. Optical frequency combs (OFC), providing many wavelengths, are particularly useful for transversal filter systems, while quantum-dash mode-locked lasers (QD-MLL), known for their ability to generate flat OFCs with low power consumption and simple operation, are promising candidates as the OFC sources. Here, we demonstrate for the first time a versatile MWP signal processor using a QD-MLL that generates an OFC with 49 comb lines and a free spectral range of 25 GHz. By tailoring the OFC spectrum, the MWP signal processor can be reconfigured to perform a variety of functions, including integral and fractional Hilbert transform (HT), differentiator, and integrator, with operation bandwidths of 7.5 GHz, 20 GHz, and 25 GHz, respectively. Owing to the large number of comb lines, the proposed HT exhibits small amplitude and phase and ripples, which are ±1.66 dB and ±6.2°, respectively, for integral HT. We also simulate the time-domain response for the different signal-processing functions based on the measured frequency responses. Our simulation and experimental results show that the QD-MLL is a promising OFC source for developing a high-speed, reconfigurable MWP processing engine.**

***Index Terms*—QD-MLL, MWP, reconfigurable signal processor.**

I. INTRODUCTION

THE rapid expansion of wireless networks, cloud-based services, and emerging artificial intelligence technologies is placing extremely high demands on the processing speed (bandwidth) of the underlying radio-frequency (RF) systems [1]. While electrical digital signal processing (DSP) technologies are well established, they face fundamental challenges in processing speed, primarily due to limitations in the electronic sampling rate. Microwave photonics (MWP) provides effective solutions for addressing these challenges by implementing signal processing in the optical domain to avoid the need for electronic sampling [2]–[6]. By leveraging the broad bandwidth and tunability provided by optical devices, MWP facilitates wideband, flexible front-end analog solutions that have the potential to outperform electrical DSPs, which are currently constrained to several gigahertz (GHz) analog bandwidths. In addition, MWP signal processors are intrinsically compatible with optical-wireless systems and can provide connectivity with in-built signal conditioning, while also featuring important advantages of electromagnetic interference (EMI) immunity.

To date, various MWP signal processors have been reported to address different types of tasks, such as reconfigurable filtering [7], [8] arbitrary waveform generation [9], [10], differenciation [11], and Hilbert transform (HT) [12]. Although wide-ranging in application, all these demonstrations are systems designed to perform a fixed function. To accommodate a broader range of scenarios, a more flexible system is necessary. One promising approach involves using a Kerr micro-comb, where each comb line serves as a delay-line tap [13]–[15]. Owing to the large number of comb lines and the flexibility of programmable optical filters, Kerr micro-comb-based MWP processing platforms potentially offer a remarkable level of reconfigurability. However, the spectrum of a Kerr micro-comb is generally non-flat, with a power difference of over 40 dB between the highest and lowest comb lines within 48 comb lines [16]. Since signal processors require a flat spectrum for efficient spectral shaping, the power available for shaping in a Kerr micro-comb is significantly low, typically limited by the lowest power comb line. Consequently, two or three erbium-doped fiber amplifiers (EDFAs) are required in Kerr micro-comb-based MWP processing platforms to compensate for the significant link loss, leading to high power consumption and system complexity. Additionally, due to spectrum flattening and multiple stages of amplification, the optical signal-to-noise ratio (OSNR) drops below 30 dB [17], which will significantly degrade the signal-to-noise ratio (SNR) in microwave signal processing. Furthermore, the requirement of careful attention to the thermal instability also increases the operation complexity. Recently, an alternative using dispersion-tailored few-mode fiber has been reported for multi-functional MWP signal processing with different modes in fiber acting as different delay-line taps [18], [19]. Processing reconfigurability can be achieved by tuning the loss of each mode through a variable optical attenuator (VOA) inserted in each line. While this method offers relatively lower power consumption, the number of delay-line taps is limited to only seven, which is not sufficient for high-performance signal processing, such

---

This work was supported in part by the Natural Sciences and Engineering Research Council of Canada. (Corresponding author: L. R. Chen) Z. Wang, Y. Xie, X. Wang, Z. Wei, J. Zhang, D. V. Plant, and L. R. Chen are with the Department of Electrical and Computer Engineering, McGill University, Montreal, QC H3A 0E9, Canada. (e-mail: zhuoran.wang5@mail.mcgill.ca; yuxuan.xie@mail.mcgill.ca; xi.wang12@mail.mcgill.ca, zixian.wei2@mail.mcgill.ca; jinsong.zhang@mail.mcgill.ca; david.plant@mcgill.ca; lawrence.chen@mcgill.ca).

J. Liu, Z. Lu, P. J. Poole, J. Weber, G. Liu, M. Rahim are with the Advanced Electronics and Photonics Research Center, National Research Council Canada, Ottawa, Ontario, ON K1A 0R6, Canada. (e-mail: jiaren.liu@nrc-cnrc.gc.ca; zhenguo.lu@nrc-cnrc.gc.ca; philip.poole@nrc-cnrc.gc.ca; john.weber@nrccnrc.gc.ca; guocheng.liu@nrc-cnrc.gc.ca; mohamed.rahim@nrc-cnrc.gc.ca;)

This article has been accepted for publication in Journal of Lightwave Technology. This is the author's version which has not been fully edited and content may change prior to final publication. Citation information: DOI 10.1109/JLT.2025.3573682

as achieving sharp phase transitions at the center frequency for fractional HT. As compared to Kerr micro-combs and dispersion-tailored few-mode fibers, QD-MLL lasers are better aligned with the needs of MWP signal processors since they provide a flatter output spectrum with less than 3 dB power difference within 58 comb lines and an OSNR greater than 40 dB [20], ensuring both sufficient power and OSNR, as well as a large number of comb lines to support efficient comb shaping [21], [22]. Additionally, the use of only DC current for pumping simplifies the operation of QD-MLLs. Moreover, the effective carrier localization property in the QDs makes them less sensitive to growth defects, allowing for the epitaxial growth of high-quality QD-MLLs on silicon, which paves the way for mass production of integrated comb sources using photonic foundry processes in the near future [23]–[25].

In this paper, we present, for the first time, a versatile MWP signal processor that uses a QD-MLL laser with 49 comb lines and a 25 GHz FSR. By tailoring the comb spectrum, our MWP signal processor is able to achieve multiple functions including integral and fractional HT, differentiation, and integration, which are basic building blocks of a general-purpose signal processor. For HT, we achieve an operation bandwidth of 7.5 GHz and characterize the RF amplitude and phase response with variable phase shifts of 15°, 30°, 45°, 60°, 75°, and 90° that correspond to fractional orders of 0.17, 0.33, 0.5, 0.67, 0.83, and 1, respectively. The amplitude and phase ripples of the 15° HT are only ± 0.15 dB and ± 3.9°, respectively. For the differentiator and integrator, the operation bandwidths are 20 GHz and 25 GHz, respectively. The integration window is simulated to be 387 ps. Time-domain simulations are conducted based on the measured frequency-domain results to verify the effectiveness of our proposed MWP signal processor. In addition to the functions presented in this paper, we have demonstrated a range of signal processing capabilities based on this QD-MLL, including a reconfigurable filter [26] and an arbitrary signal generator [27]. Not least among these functions, theoretically, all types of processing functions based on FIR filters with real-valued taps can be implemented owing to the powerful programmability of the optical filter and the large number of usable comb lines from the QD-MLL. This makes our approach a promising solution for implementing high-speed, reconfigurable signal processors.

II. PRINCIPLE OF OPERATION

The fundamental principle is to transform the continuous impulse response of a specific function into a truncated discrete response so that the transfer function can be expressed by a finite impulse response (FIR) filter as

$$H(\omega)=\sum_{n=0}^{N-1} h[n] e^{-j\omega n\Delta t} \tag{1}$$

where $h[n]$ is the discrete impulse response, which also corresponds to the coefficient of the delay-line tap, Δt is the time delay between adjacent taps, and N is the total number of taps. As Eq. 1 is the discrete version of the ideal temporal impulse response of a specific function, the corresponding frequency response is periodic and bandwidth-limited with the first null frequency located at

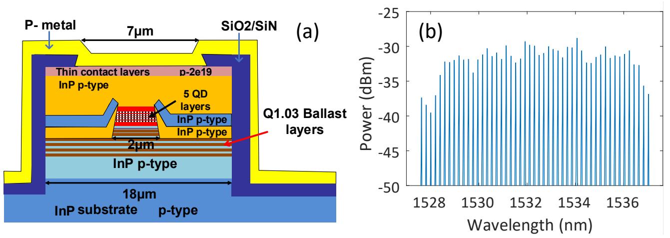

Fig. 1. (a) QD laser's structure. (b) QD laser's output spectrum at a pump current of 220 mA and a temperature of 28°C.

$$f_c=\frac{1}{\Delta t} \tag{2}$$

To implement the specific function, each comb line from the QD-MLL serves as an optical carrier of a microwave delay-line tap. The power of the nth comb line is weighted according to the coefficient of the nth tap of impulse response $h_P[n]$. The time delay between adjacent taps is introduced by a dispersive medium, such as a length of optical fiber. According to Eq. 2, the first null frequency will be located at $f_c = 1/(D\Delta\lambda)$, where D is the group velocity dispersion (GVD) and $\Delta\lambda$ is the wavelength spacing between adjacent comb lines. Finally, all the taps are summed together by a photodetector (PD) to generate the RF output. To reconfigure the signal processor, we can properly adjust the tap coefficients accordingly, namely the power of each comb line, through a programmable optical filter. However, certain signal processing functions, such as the HT or differentiators, require negative tap coefficients. Since optical power cannot be negative, a balanced photodetector (BPD) is employed to achieve negative tap coefficients by injecting taps with opposite signs into separate ports of the BPD.

We utilize an InAs/InP-based QD-MLL as the OFC source, with its cross-section shown in Fig. 1(a). The core of the QD laser consists of a 350 nm InGaAsP layer containing five layers InAs quantum dot (QD) with a periodicity of 108 Å, surrounded by a p-type InP cladding. Additional physical details of this laser can be found in [20], [28]. The threshold current for this QD laser is approximately 50 mA. The QD laser supports mode-locked operation with a nearly flat comb spectrum when the pump current exceeds 200 mA. For our experiments, we operate the laser at a current of approximately 220 mA and a temperature of 28°C, which generates 49 comb lines in the C-band with a 25 GHz (0.2 nm) spacing, as shown in Fig. 1(b).

A. Hilbert Transformer

The ideal frequency response of a fractional HT (FHT) can be expressed as [29]

$$H_P(\omega)=\begin{cases} e^{-j\varphi}, & 0\le\omega<\pi \\ e^{j\varphi}, & -\pi\le\omega<0 \end{cases} \tag{3}$$

where $\varphi = P\times\pi/2$ is the phase shift, with P denoting the fractional order. Its frequency response is plotted in Fig. 2(a).

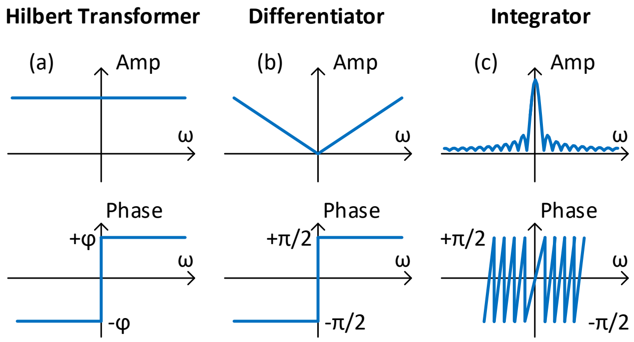

Fig. 2. Ideal frequency responses of (a) HT; (b) differentiator; (c) integrator.

At zero frequency, there will be a phase jump of φ. As can be seen, an FHT can be regarded as a phase shifter with a phase shift of φ around the center frequency ω. When $P = 1$, it becomes an integral HT with a phase shift of 90 degrees. The corresponding discrete-time impulse response is given by [30]

$$h_P[n] = \begin{cases} \sin(\varphi) \cdot \frac{2}{\pi} \cdot \frac{\sin^2(\pi n/2)}{n}, & n \neq 0 \\ \cos(\varphi), & n = 0 \end{cases} \tag{4}$$

B. Differentiator

The ideal frequency response of a differentiator can be expressed as

$$H_D(\omega) = j\omega \tag{5}$$

where $j = \sqrt{-1}$. Its frequency response is plotted in Fig. 2(b). At zero frequency, there will be a phase jump of π. For differentiators, there is no analytical expression of the corresponding impulse response. The tap coefficients are calculated using the Remez algorithm [31].

C. Integrator

Different from HT and differentiation, the realization of the integrator is based on the delay-sum principle as [32], [33]

$$y(t) = \sum_{n=0}^{N-1} x(t - n \cdot \Delta t) \tag{6}$$

where $x(t)$ is the input RF signal and $y(t)$ is the output RF signal from the PD. Its frequency response is plotted in Fig. 2(c). At zero frequency, the phase is continuous, while at null frequencies, there are phase jumps of π. According to Eq. 6, the tap coefficients are all 1, thereby the comb should have a flat spectrum. After the replicas of $x(t)$ are delayed progressively and summed together, the integration function can be achieved, with a time feature of Δt, an operation bandwidth of $1/\Delta t$, and a total integration time window of $T = N \cdot \Delta t$ [32].

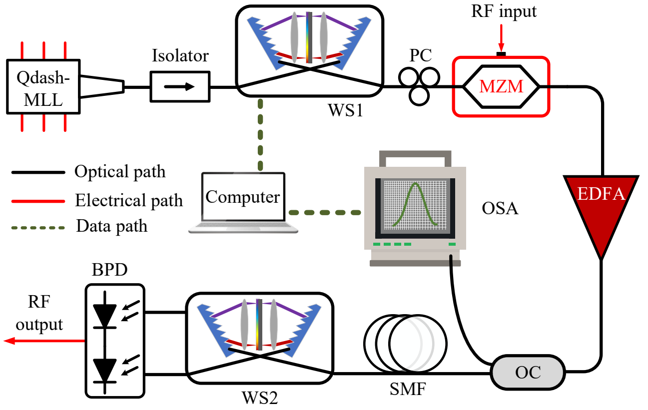

Fig. 3. Schematic diagram of our proposed MWP signal processor. WS: Waveshaper; PC: polarization controller; MZM: Mach-Zehnder modulator; SMF: single-mode fiber; EDFA: erbium-doped fiber amplifier; BPD: balanced photodetector; OSA: optical spectrum analyzer.

III. EXPERIMENTAL DEMONSTRATION

The schematic of the proposed signal processor is shown in Fig. 3. The OFC with 49 comb lines generated by the QD-MLL is first reshaped using a programmable optical filter (FINISAR, WaveShaper 1000S) to match the desired tap coefficients, with an isolator inserted in between to prevent backscattering. Then the reshaped light is directed to the Mach-Zehnder modulator (MZM) (AVANEX, SD40) for modulation by the RF signal. A polarization controller (PC) is used to align the polarization to the MZM. After that, an EDFA (KEOPSYS, CEFA-C-BO-HP) is used to compensate for the net loss. 10% of the reshaped optical signal is coupled out and directed to an optical spectrum analyzer (OSA) (AQ6317) for feedback control. Since the EDFA is placed after Waveshaper 1000S, which causes spectrum distortion, a feedback loop is used to compensate for the tap coefficient error, achieved by comparing the monitored results from the OSA with the desired channel weights, generating an error signal that is used to adjust the loss characteristics of the Waveshaper. Fig. 4 compares the coefficient accuracy for the integral HT with and without the feedback loop. Without the feedback loop, the maximum coefficient error is 2.1 dB, whereas with the feedback loop, the maximum error is reduced to 0.7 dB. Notably, the feedback control is not real-time due to the limited update speed of the Waveshaper, which takes a few seconds. The Waveshaper (WS1) is fixed once a relatively accurate spectrum is obtained. Typically, the feedback process is repeated two to three times before it converges and stops. The main error originates from the power instability of the comb source, which fluctuates within 0.5 dB, and from the shaping inaccuracies of the Waveshaper. The latter can be well mitigated by adopting self-calibrating programmable photonic integrated circuits [34]. The remaining 90 percent of the signal passes through a length (10 km or 2 km of single-mode fiber (SMF) which provides the necessary delay to realize the signal processing function, followed by another optical programmable filter (FINISAR, WaveShaper 4000S) used for 1) splitting the positive taps and negative taps into

This article has been accepted for publication in Journal of Lightwave Technology. This is the author's version which has not been fully edited and
content may change prior to final publication. Citation information: DOI 10.1109/JLT.2025.3573682

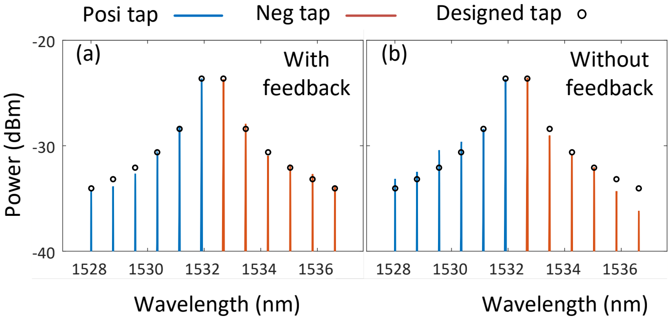

Fig. 4. Experimental optical spectrum of 90° HT with feedback loop (a), without feedback loop (b).

two paths and 2) removing the ASE noise floor between each taps. In principle, the first Waveshaper is redundant, as the second Waveshaper can perform all necessary tasks, including spectrum shaping, tap splitting, and ASE removal. Finally, the positive taps and negative taps are detected by two ports of a BPD (Finisar, BPDV21x0R) to generate the RF output signal. The frequency response is measured by a vector network analyzer (VNA) (Keysight, N5225A).

To achieve the HT, 10 km of SMF was used. The comb spacing was adjusted to 50 GHz (0.4 nm) by selecting one in two comb lines. As a result, the first null frequency was located at around 7.5 GHz. Since the center tap coefficient is zero for the integral HT, its comb spacing is 100 GHz (0.8 nm). It is worth mentioning that the bandwidth can be extended up to 25 GHz, which is the half of the comb spacing, by using a proper length of fiber. Moreover, by selecting one of the four comb lines, which increases the comb spacing by a factor of four, the bandwidth can potentially reach 50 GHz. Fig. 5(a-i)-(a-vi) show the optical spectra for the fractional HT with different orders of 0.166, 0.333, 0.5, 0.667, 0.833, 1, corresponding to phase shifts of 15°, 30°, 45°, 60°, 75°, 90°. The blue line and red line represent positive taps and negative taps, respectively, while the black circles represent the designed tap coefficients. As shown, a good match between the power of the measured comb lines and the calculated ideal tap coefficients was obtained, indicating that the comb lines were accurately shaped. Fig. 5(b-i)-(b-vi) and (c-i)-(c-vi) present the measured magnitude and phase responses, respectively. The blue traces represent the frequency response calculated using the ideal tap coefficients obtained using Eq. 4. To investigate the effect of tap coefficient errors, we also calculated the frequency response using the tap coefficients obtained by the experiment, namely the power of the comb lines. We refer this to quasi-ideal result, represented by the red traces. As shown, the ideal and quasi-ideal frequency responses almost overlap, indicating a negligible effect from the tap coefficient error. With the influence of the tap coefficient error ruled out, the non-ideal experimental frequency responses (yellow traces) are primarily due to the non-uniform optical loss for each tap and nonlinear dispersion, which can be resolved by implementing pre-compensation to the OFC in the future [13], [35]. The amplitude and phase ripples for different orders of HT are summarized in Table I. Due to the lack of a real-time oscilloscope, the time-domain results were obtained in simulation using the measured frequency response. The input Gaussian pulse has a pulse width of 0.15 ns corresponding to 3 GHz bandwidth, represented by the black line in Fig. 5(d-i). The output pulses simulated using measured frequency responses are plotted in Fig. 5(d-i)-(d-vi), represented by the blue traces. For comparison, the ideal output pulses (red dash traces) simulated using the ideal frequency responses are also plotted. As can be seen, the simulated time-domain results match well with the expected ideal results, verifying the effectiveness of our signal processor. The root-mean-square errors (RMSEs) between the simulated and theoretical curves are 1.72%, 1.55%, 1.48%, 1.71%, 1.65%, 1.84% for the 90° HT through to the 15° HT, respectively.

TABLE I
PERFORMANCE OF THE SIGNAL PROCESSOR

Function	Amplitude ripple	Phase ripple	Bandwidth	RMSE
90° HT	±1.66 dB	±6.2°	7.5 GHz	1.72%
75° HT	±1.54 dB	±4.1°	7.5 GHz	1.55%
60° HT	±0.77 dB	±4.3°	7.5 GHz	1.48%
45° HT	±0.28 dB	±4.5°	7.5 GHz	1.71%
30° HT	±0.29 dB	±4.1°	7.5 GHz	1.65%
15° HT	±0.15 dB	±3.9°	7.5 GHz	1.84%
Differentiator	None	None	20 GHz	5.17%
Integrator	None	None	25 GHz	2.04%

To achieve the differentiator and integrator functions, 2 km SMF was used. The comb spacing remained at 50 GHz. As a result, the first null frequency was located at around 37.5 GHz. For the differentiator, the operation bandwidth we achieved is 20 GHz. Ideally, the maximum achievable bandwidth for the differentiator should be half of the comb spacing. However, it failed to reach the theoretical maximum value because an accurate comb-splitting process is required to separate positive and negative taps. As shown in Fig. 7(a), positive and negative taps alternate with each other, which are calculated using the Remez algorithm. In order to split the taps, the optical windowing filter's edge should be accurately placed in the center between positive and negative taps. Once there is an offset, the operation bandwidth will be reduced by the optical windowing filter, as shown in Fig. 6. As a result, the real bandwidth equals to half of the comb spacing minus the offset Δ. To alleviate this bandwidth reduction, a careful optimization process on the offset should be implemented, while the filter's edge should be as sharp as possible. The magnitude response of the differentiator is plotted in Fig. 7(b) with the linear scaled magnitude response inserted, which verifies the good match between measured results and theoretical results. For the phase response, a phase ripple of ± 0.35 rad is observed, as shown in Fig. 7(c), which cause a relatively large RMSE of 5.17% in time-domain simulation as depicted in Fig. 7(d). The input Gaussian pulse in the simulation has a width of 22 ps, corresponding to a bandwidth of 20 GHz. For the integrator, the comb spectrum is flattened and all taps are positive as shown in Fig. 7(e). The achieved operational bandwidth is 25 GHz, primarily limited by the bandwidth of the RF amplifier

This article has been accepted for publication in Journal of Lightwave Technology. This is the author's version which has not been fully edited and content may change prior to final publication. Citation information: DOI 10.1109/JLT.2025.3573682

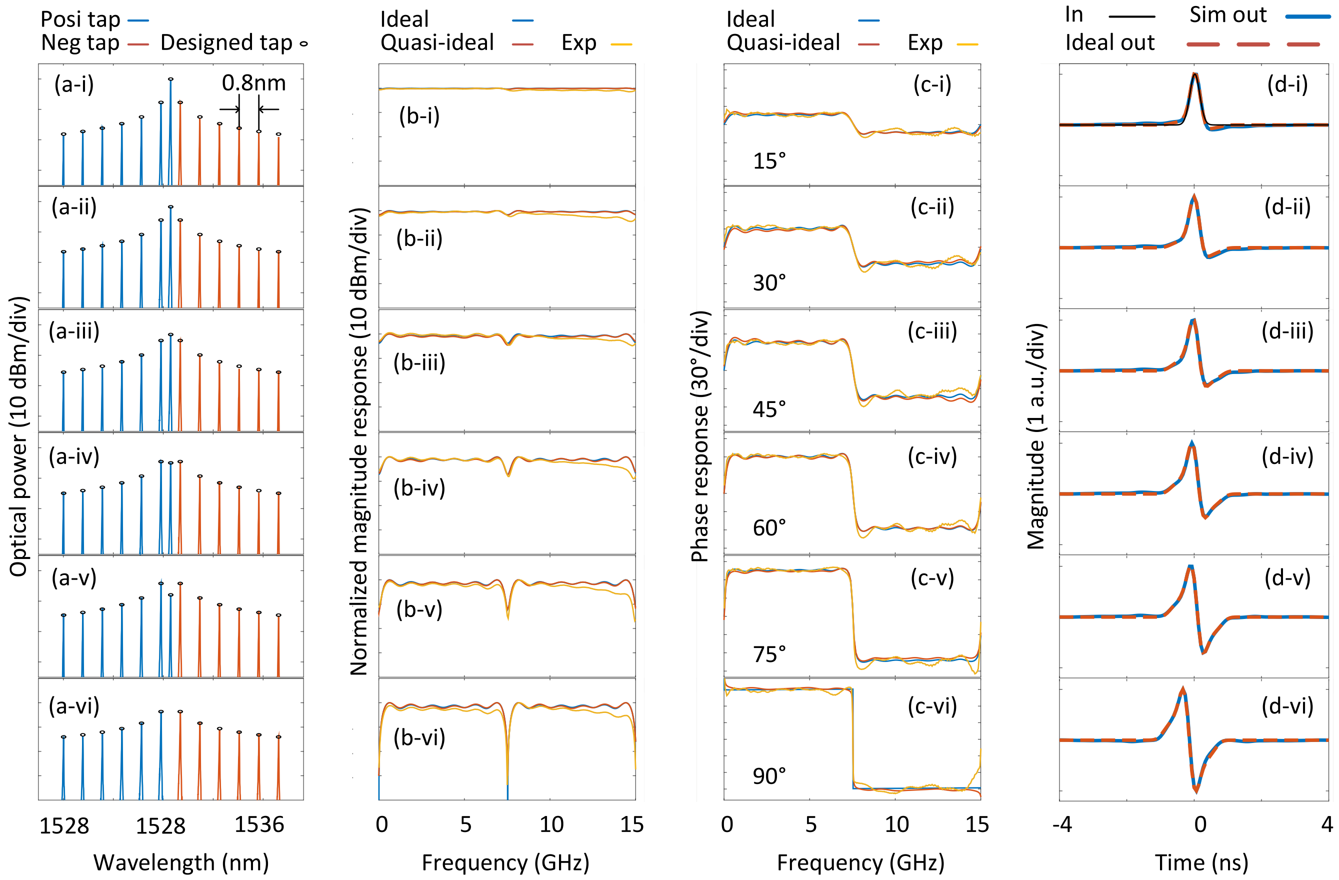

Fig. 5. (a-i)-(a-vi) Experimental optical spectra associated with 15°, 30°, 45°, 60°, 75°, 90° HT. (b-i)-(b-vi) Corresponding normalized magnitude responses. (c-i)-(c-vi) Corresponding phase responses in degree. (d-i)-(d-vi) Corresponding time-domain simulation results.

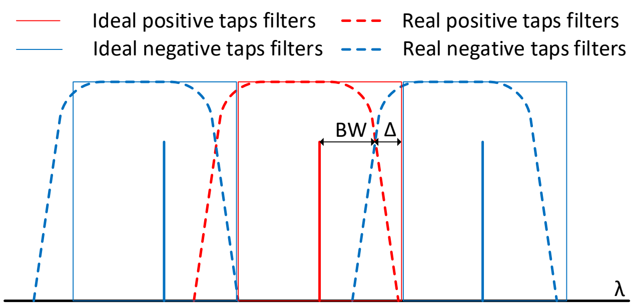

Fig. 6. Illustration of bandwidth reduction in the differentiator due to optical filter offset.

(SHF P101) used to boost the output signal. In the phase response, a phase error of approximately 1 rad is observed in the frequency range from 17 GHz to 19.5 GHz. Due to the fundamental difference between the differentiator and the integrator, where the latter is based on the delay-sum principle and relies solely on the taps' intensity, the phase response error of the integrator does not significantly affect its time-domain performance. In the time-domain simulation for the integrator, we used an 18 ps Gaussian pulse as input corresponding to 25 GHz bandwidth. As shown in Fig. 7(h), an integration window of 387 ps is achieved, matching well with the theoretical value of $N \cdot \Delta t$ with N being 25 and Δt being 13.6 ps = 0.4 nm × 2 km × 17 ps/nm/km. The RMSE of the integrator is calculated to be 2.04%.

Lastly, we investigated the impact of third-order dispersion (TOD) on the performance of the implemented functions through simulation. In reality, fiber dispersion is typically not constant; it varies with wavelength, which is referred to as the TOD or dispersion slope. This variation means that the time delay between adjacent taps is not uniform. When the optical bandwidth or the fiber length increases, the differences in time delay also increase, which will cause non uniformly distributed delay-line taps. Here, we compare three different values of TOD, S = 0, 0.05, and 0.1 ps/km/nm^2. Note that the typical value of S for a commercial SMF is around 0.05 ps/km/nm^2. As shown in Fig. 8(d), a larger value of S leads to more pronounced phase ripples in the Hilbert transformer. In the case of the differentiator, stronger nonlinear phase deviations are observed at higher frequencies, particularly above 25 GHz. For the integrator, TOD induces a negligible nonlinear phase response, but instead reduces the period of the sidelobes — an effect equivalent to that of additional dispersion. Despite these imperfections in the phase response, the time-domain signal profiles remain largely unaffected by variations in S in all cases. For instance, in the case of the differentiator, since the intended operating frequencies are below 20 GHz,

This article has been accepted for publication in Journal of Lightwave Technology. This is the author's version which has not been fully edited and content may change prior to final publication. Citation information: DOI 10.1109/JLT.2025.3573682

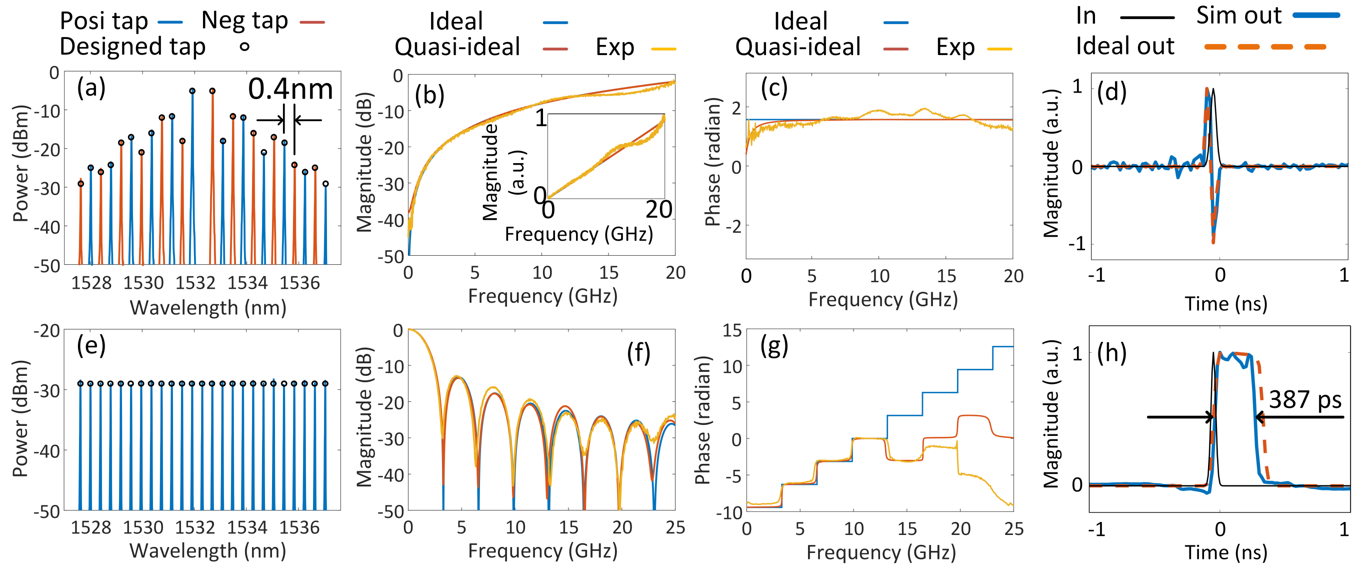

Fig. 7. (a)(e) Experimental optical spectra associated with the differentiator and integrator, respectively. (b)(f) Corresponding normalized magnitude responses. (c)(g) Corresponding phase responses in degrees. (d)(h) Corresponding time-domain simulation results.

the nonlinear phase distortion at higher frequencies has no practical influence on performance.

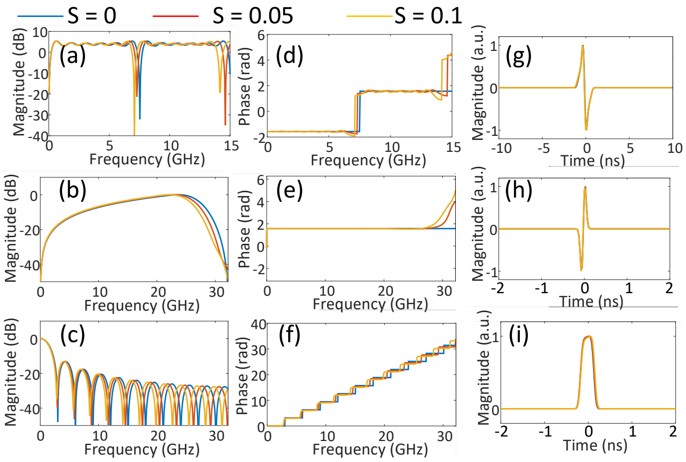

Fig. 8. Investigation of the effect of TOD: (a–c) simulated amplitude responses of the Hilbert transformer, differentiator, and integrator, respectively; (d–f) corresponding simulated phase responses; (g–i) simulated time-domain profiles for the Hilbert transformer, differentiator, and integrator, respectively.

A comprehensive comparison between the proposed signal processor and other previously reported works has been added, as given in Table II. As can be seen, we are the first to include all the building-block signal processing functions. Theoretically, our QD-MLL-based signal processor can be reconfigured to implement any FIR filter with real-valued tap coefficients. Furthermore, FIR filters with complex tap coefficients could potentially be realized by adopting single-sideband modulation (SSB) [38], leveraging the phase manipulation capabilities of the Waveshaper. This is because, under SSB modulation, the phase of the optical carrier directly maps to the phase of the resulting RF signal. Consequently, by precisely controlling the optical carrier's phase through the Waveshaper, we can effectively manipulate the phase of each tap, enabling the implementation of complex-valued FIR filtering. Alternatively, complex-valued taps can also be achieved using non-uniformly distributed tap delays, which can be implemented by applying user-defined group delays to individual taps via the Waveshaper [39]. Additionally, we achieved smallest magnitude ripples of ± 1.7 dB, owing to a large number of available comb lines, while the phase ripple is relatively large due to a combination of factors, including an non-flat system response to different wavelengths, BPD's imbalance to positive and negative taps, TOD, and power instability from QD-MLL. Regarding bandwidth, the 7.5 GHz demonstrated here is not the upper limit of the QD-MLL-based signal processor. By shortening the fiber length, the bandwidth can be extended to nearly half of the comb spacing. This principle also applies to Kerr-comb-based signal processors. More importantly, compared to Kerr-comb-based signal processors, our approach requires fewer EDFAs owing to the flat optical spectrum of the QD-MLL, ensuring sufficient OSNR. Given the flatness of the spectrum produced by the QD-MLL and the power of each comb line approaching 0 dBm, the EDFA in our setup can potentially be replaced by an electrical amplifier (EA), which is more integration-friendly, provided the link loss is fully optimized. This substitution not only simplifies the system architecture but also greatly enhances its compatibility with monolithic integration. In contrast, Kerr-comb-based systems inherently require EDFAs to boost the low optical power, which is a critical bottleneck that poses serious challenges for scalable, on-chip photonic integration.

IV. CONCLUSION

In conclusion, we first time demonstrate a QD-MLL-based versatile MWP signal processor. By tailoring the OFC spectrum, the processor achieves multiple reconfigurable functions, including integral and fractional HT, differentiation,

This article has been accepted for publication in Journal of Lightwave Technology. This is the author's version which has not been fully edited and content may change prior to final publication. Citation information: DOI 10.1109/JLT.2025.3573682

TABLE II
PERFORMANCE COMPARISON OF MWP SIGNAL PROCESSORS

Ref	Approach	DIFF	INT	HT	FHT	BW (GHz)	OSNR (dB)	Power Consumption	HT Amplitude Ripples (dB)	HT Phase Ripples (°)
[11]	Discrete tunable lasers	✓	-	-	-	2	40	1 EDFA	N/A	N/A
[36]	Discrete tunable lasers	-	-	✓	✓	4.5	N/A	1 EDFA	$\sim \pm 5$	± 5
[37]	ASE source	✓	-	-	-	25	N/A	1 EDFA	N/A	N/A
[32]	ASE source	-	✓	-	-	9.6	N/A	0 EDFA	N/A	N/A
[18]	Multicore fiber	-	-	✓	✓	3.2	N/A	2 EDFA	$> \pm 5$	±5.9
[19]	Multicore fiber	✓	✓	-	-	N/A	N/A	1 EDFA	N/A	N/A
[14]	Kerr comb	✓	-	-	-	8.5	30	2 EDFA	N/A	N/A
[13]	Kerr comb	-	✓	-	-	11.9	20	3 EDFA	N/A	N/A
[15]	Kerr comb	-	-	✓	✓	16.5	> 20	3 EDFA	± 2.9	± 4
This work	**QD-MLL**	✓	✓	✓	✓	**7.5 (HT)**	**40**	**1 EDFA**	**± 1.7**	**± 6.2**

Notes: "-" represents not reported; "✓" represents achieved; "N/A" represents that the values were not explicitly provided or could not be extracted from the available results. DIFF: differentiator; INT: integrator.

and integration. It is worth mentioning that our platform is not limited to just these three functions, but can also realize all FIR filter-based functions, provided the tap values are real. The QD-MLL's relatively flat output spectrum and large number of comb lines, as well as the high OSNR, provide significant advantages over existing technologies like Kerr micro-combs or multi-core fibers. These features enable efficient spectral shaping, reduced system complexity, and lower power consumption while maintaining high-speed processing capabilities. Although the system currently is bulky and expensive since two Waveshapers are used, it is promising to realize a fully integrated MWP signal processor with heterogeneously integrating the QD-MLL onto a SOI platform, the Waveshapers being replaced by on-chip programmable spectral shapers [9], [40], and long SMF being replaced by on-chip multichannel chirped FBGs [41], [42] or sub-wavelength gratings [43], [44], the back-reflections being minimized by angled facets or on-chip isolator [45]. Therefore, combining QD-MLLDs with advanced silicon photonic devices offers an attractive path toward robust and technically simple chip-scale MWP signal processing platforms. Once fully integrated, the proposed MWP signal processor is anticipated to play a key role in autonomous driving systems, where high-speed and real-time signal processing—such as edge detection—is highly demanded.

REFERENCES

[1] V. Ilderem, "The technology underpinning 5G," *Nature Electronics*, vol. 3, pp. 5–6, 2020.

[2] H. Feng, T. Ge, X. Guo *et al.*, "Integrated lithium niobate microwave photonic processing engine," *Nature*, vol. 627, pp. 80–87, 2024.

[3] W. Liu, M. Li, R. Guzzon *et al.*, "A fully reconfigurable photonic integrated signal processor," *Nature Photonics*, vol. 10, pp. 190–195, 2016.

[4] R. A. Minasian, E. H. W. Chan, and X. Yi, "Microwave photonic signal processing," *Opt. Express*, vol. 21, no. 19, pp. 22 918–22 936, 2013.

[5] L. Zhuang, C. G. H. Roeloffzen, M. Hoekman, K.-J. Boller, and A. J. Lowery, "Programmable photonic signal processor chip for radiofrequency applications," *Optica*, vol. 2, no. 10, pp. 854–859, 2015.

[6] M. Tan, X. Xu, A. Boes *et al.*, "Photonic signal processor based on a Kerr microcomb for real-time video image processing," *Communications Engineering*, vol. 2, p. 94, 2023.

[7] X. Xu, M. Tan, J. Wu, T. G. Nguyen, S. T. Chu, B. E. Little, R. Morandotti, A. Mitchell, and D. J. Moss, "Advanced adaptive photonic RF filters with 80 taps based on an integrated optical micro-comb source," *Journal of Lightwave Technology*, vol. 37, no. 4, pp. 1288–1295, 2019.

[8] J. Hu, J. He, J. Liu *et al.*, "Reconfigurable radiofrequency filters based on versatile soliton microcombs," *Nature Communications*, vol. 11, no. 1, p. 4377, 2020.

[9] M. Khan, H. Shen, Y. Xuan *et al.*, "Ultrabroad-bandwidth arbitrary radiofrequency waveform generation with a silicon photonic chip-based spectral shaper," *Nature Photonics*, vol. 4, pp. 117–122, 2010.

[10] J. Wang, H. Shen, L. Fan *et al.*, "Reconfigurable radio-frequency arbitrary waveforms synthesized in a silicon photonic chip," *Nature Communications*, vol. 6, p. 5957, 2015.

[11] Y. Han, Z. Li, and J. Yao, "A microwave bandpass differentiator implemented based on a nonuniformly-spaced photonic microwave delay-line filter," *Journal of Lightwave Technology*, vol. 29, no. 22, pp. 3470–3475, 2011.

[12] M. Li and J. Yao, "All-fiber temporal photonic fractional Hilbert transformer based on a directly designed fiber Bragg grating," *Opt. Lett.*, vol. 35, no. 2, pp. 223–225, 2010.

[13] X. Xu, M. Tan, J. Wu, A. Boes, B. Corcoran, T. G. Nguyen, S. T. Chu, B. E. Little, R. Morandotti, A. Mitchell, and D. J. Moss, "Photonic RF and microwave integrator based on a transversal filter with soliton crystal microcombs," *IEEE Transactions on Circuits and Systems II: Express Briefs*, vol. 67, no. 12, pp. 3582–3586, 2020.

[14] X. Xu, J. Wu, M. Shoeiby, T. G. Nguyen, S. T. Chu, B. E. Little, R. Morandotti, A. Mitchell, and D. J. Moss, "Reconfigurable broadband microwave photonic intensity differentiator based on an integrated optical frequency comb source," *APL Photonics*, vol. 2, no. 9, p. 096104, 2017.

[15] M. Tan, X. Xu, B. Corcoran, J. Wu, A. Boes, T. G. Nguyen, S. T. Chu, B. E. Little, R. Morandotti, A. Mitchell, and D. J. Moss, "Microwave and RF photonic fractional Hilbert transformer based on a 50 GHz Kerr micro-comb," *Journal of Lightwave Technology*, vol. 37, no. 24, pp. 6097–6104, 2019.

[16] X. Xue, Y. Xuan, C. Bao, S. Li, X. Zheng, B. Zhou, M. Qi, and A. M. Weiner, "Microcomb-based true-time-delay network for microwave beamforming with arbitrary beam pattern control," *Journal of Lightwave Technology*, vol. 36, no. 12, pp. 2312–2321, 2018.

[17] X. Xu, J. Wu, T. G. Nguyen, M. Shoeiby, S. T. Chu, B. E. Little, R. Morandotti, A. Mitchell, and D. J. Moss, "Advanced RF and microwave functions based on an integrated optical frequency comb source," *Opt. Express*, vol. 26, no. 3, pp. 2569–2583, 2018.

[18] E. Nazemosadat and I. Gasulla, "Microwave fractional Hilbert transformer implemented in a dispersion-tailored few-mode fiber," *Opt. Express*, vol. 32, no. 12, pp. 20 528–20 537, 2024.

[19] S. García and I. Gasulla, "Photonic temporal operators for microwave signals enabled by multicore fibers," *Journal of Lightwave Technology*, vol. 42, no. 21, pp. 7596–7603, 2024.

[20] Z. Lu, J. Liu, P. J. Poole, Y. Mao, J. Weber, G. Liu, and P. Barrios, "InAs/InP quantum dash semiconductor coherent comb lasers and their applications in optical networks," *Journal of Lightwave Technology*, vol. 39, no. 12, pp. 3751–3760, 2021.

[21] Y. Xie, G. Liu, J. Liu, Z. Lu, P. J. Poole, J. Weber, P. Barrios, M. Rahim, and L. R. Chen, "A heterodyne detection based photonic-assisted ADC using quantum dash mode-locked laser," in *2024 International Topical Meeting on Microwave Photonics (MWP)*, 2024, pp. 1–4.

[22] G. Liu, P. J. Poole, Z. Lu, J. Liu, C.-Y. Song, Y. Mao, and P. Barrios, "Mode-locking and noise characteristics of InAs/InP quantum dash/dot

lasers," *Journal of Lightwave Technology*, vol. 41, no. 13, pp. 4262–4270, 2023.

[23] S. Liu, X. Wu, D. Jung, J. C. Norman, M. J. Kennedy, H. K. Tsang, A. C. Gossard, and J. E. Bowers, "High-channel-count 20 Ghz passively mode-locked quantum dot laser directly grown on Si with 4.1 Tbit/s transmission capacity," *Optica*, vol. 6, no. 2, pp. 128–134, 2019.

[24] L. Chang, S. Liu, and J. Bowers, "Integrated optical frequency comb technologies," *Nature Photonics*, vol. 16, pp. 95–108, 2022.

[25] Y. De Koninck, C. Caer, D. Yudistira *et al.*, "Gaas nano-ridge laser diodes fully fabricated in a 300-mm CMOS pilot line," *Nature*, vol. 637, pp. 63–69, 2025.

[26] H. Sun, M. Khalil, J. Liu, Z. Lu, P. J. Poole, J. Weber, D. V. Plant, and L. R. Chen, "Reconfigurable microwave photonic filter based on a quantum dash mode-locked laser," *Opt. Lett.*, vol. 47, no. 5, pp. 1133–1136, 2022.

[27] Y. Xie, M. Khalil, T. Erfan, J. Liu, Z. Lu, P. J. Poole, J. Weber, G. Liu, M. Rahim, and L. R. Chen, "Arbitrary waveform generation system using a quantum dash optical frequency comb source," *Opt. Continuum*, vol. 3, no. 8, pp. 1291–1301, 2024.

[28] G. Liu, Z. Lu, J. Liu, P. J. Poole, Y. Mao, K. Zeb, X. Xie, M. Vachon, P. Barrios, C.-y. Song, N. Sabourin, J. Weber, X. Zhang, K. Wu, and J. Yao, "Monolithic InAs/InP quantum dash mode-locked lasers for millimeter-wave-over-fiber mobile fronthaul systems," *IEEE Journal of Selected Topics in Quantum Electronics*, vol. 29, no. 6: Photonic Signal Processing, pp. 1–10, 2023.

[29] A. W. Lohmann, D. Mendlovic, and Z. Zalevsky, "Fractional Hilbert transform," *Opt. Lett.*, vol. 21, no. 4, pp. 281–283, 1996.

[30] C.-C. Tseng and S.-C. Pei, "Design and application of discrete-time fractional Hilbert transformer," *IEEE Transactions on Circuits and Systems II: Analog and Digital Signal Processing*, vol. 47, no. 12, pp. 1529–1533, 2000.

[31] J. McClellan, T. Parks, and L. Rabiner, "A computer program for designing optimum FIR linear phase digital filters," *IEEE Transactions on Audio and Electroacoustics*, vol. 21, no. 6, pp. 506–526, 1973.

[32] Y. Park and J. A. na, "Ultrafast photonic intensity integrator," *Opt. Lett.*, vol. 34, no. 8, pp. 1156–1158, 2009.

[33] M. H. Asghari, Y. Park, and J. A. na, "Photonic temporal integration of broadband intensity waveforms over long operation time windows," *Opt. Lett.*, vol. 36, no. 18, pp. 3557–3559, 2011.

[34] X. Xu, G. Ren, T. Feleppa *et al.*, "Self-calibrating programmable photonic integrated circuits," *Nature Photonics*, vol. 16, pp. 595–602, 2022.

[35] X. Yi, T. X. H. Huang, L. Li, and R. A. Minasian, "Overcoming tap-delay-variation induced distortion in microwave photonic filters," *IEEE Photonics Technology Letters*, vol. 24, no. 8, pp. 691–693, 2012.

[36] Z. Li, Y. Han, H. Chi, X. Zhang, and J. Yao, "A continuously tunable microwave fractional hilbert transformer based on a nonuniformly spaced photonic microwave delay-line filter," *Journal of Lightwave Technology*, vol. 30, no. 12, pp. 1948–1953, 2012.

[37] Y. Park, M. H. Asghari, R. Helsten, and J. Azana, "Implementation of broadband microwave arbitrary-order time differential operators using a reconfigurable incoherent photonic processor," *IEEE Photonics Journal*, vol. 2, no. 6, pp. 1040–1050, 2010.

[38] M. Sagues, R. G. Olcina, A. Loayssa, S. Sales, and J. Capmany, "Multi-tap complex-coefficient incoherent microwave photonic filters based on optical single-sideband modulation and narrow band optical filtering," *Opt. Express*, vol. 16, no. 1, pp. 295–303, 2008.

[39] Y. Dai and J. Yao, "Nonuniformly spaced photonic microwave delay-line filters and applications," *IEEE Transactions on Microwave Theory and Techniques*, vol. 58, no. 11, pp. 3279–3289, 2010.

[40] L. Cohen, K. Wu, K. Myilswamy *et al.*, "Silicon photonic microresonator-based high-resolution line-by-line pulse shaping," *Nat Commun*, vol. 15, p. 7878, 2024.

[41] J. Zhang and J. Yao, "Microwave photonic integrator based on a multichannel fiber Bragg grating," *Opt. Lett.*, vol. 41, no. 2, pp. 273–276, 2016.

[42] M. Burla, L. R. Cortés, M. Li, X. Wang, L. Chrostowski, and J. A. na, "Integrated waveguide Bragg gratings for microwave photonics signal processing," *Opt. Express*, vol. 21, no. 21, pp. 25 120–25 147, 2013.

[43] Y. Wang, H. Sun, M. Khalil, W. Dong, I. Gasulla, J. Capmany, and L. R. Chen, "On-chip optical true time delay lines based on subwavelength grating waveguides," *Opt. Lett.*, vol. 46, no. 6, pp. 1405–1408, 2021.

[44] H. Sun, Y. Wang, and L. R. Chen, "Integrated discretely tunable optical delay line based on step-chirped subwavelength grating waveguide Bragg gratings," *Journal of Lightwave Technology*, vol. 38, no. 19, pp. 5551–5560, 2020.

[45] Y. Zhang, Q. Du, C. Wang, T. Fakhrul, S. Liu, L. Deng, D. Huang, P. Pintus, J. Bowers, C. A. Ross, J. Hu, and L. Bi, "Monolithic integration of broadband optical isolators for polarization-diverse silicon photonics," *Optica*, vol. 6, no. 4, pp. 473–478, 2019.